

Modeling and Performance Analysis for Movable Antenna Enabled Wireless Communications

Lipeng Zhu, *Member, IEEE*, Wenyan Ma, *Student Member, IEEE*, and Rui Zhang, *Fellow, IEEE*

Abstract

In this paper, we propose a novel antenna architecture called movable antenna (MA) to improve the performance of wireless communication systems. Different from conventional fixed-position antennas (FPAs) that undergo random wireless channel variation, the MAs with the capability of flexible movement can be deployed at positions with more favorable channel conditions to achieve higher spatial diversity gains. To characterize the general multi-path channel in a given region or field where the MAs are deployed, a field-response model is developed by leveraging the amplitude, phase, and angle of arrival/angle of departure (AoA/AoD) information on each of the multiple channel paths under the far-field condition. Based on this model, we then analyze the maximum channel gain achieved by a single receive MA as compared to its FPA counterpart in both deterministic and stochastic channels. First, in the deterministic channel case, we show the periodic behavior of the multi-path channel gain in a given spatial field, which can be exploited for analyzing the maximum channel gain of the MA. Next, in the case of stochastic channels, the expected value of an upper bound on the maximum channel gain of the MA in an infinitely large receive region is derived for different numbers of channel paths. The approximate cumulative distribution function (CDF) for the maximum channel gain is also obtained in closed form, which is useful to evaluate the outage probability of the MA system. Moreover, our results reveal that higher performance gains by the MA over the FPA can be acquired when the number of channel paths increases due to more pronounced small-scale fading effects in the spatial domain. Numerical examples are presented which validate our analytical results and demonstrate that the MA system can reap considerable performance gains over the conventional FPA systems with/without antenna selection (AS), and even achieve comparable performance to the single-input multiple-output (SIMO) beamforming system.

Index Terms

Movable antenna (MA), spatial diversity, field response, performance analysis.

L. Zhu and W. Ma are with the Department of Electrical and Computer Engineering, National University of Singapore, Singapore 117583 (e-mail: zhulp@nus.edu.sg, wenyan@u.nus.edu).

R. Zhang is with The Chinese University of Hong Kong, Shenzhen, and Shenzhen Research Institute of Big Data, Shenzhen, China 518172 (e-mail: rzhang@cuhk.edu.cn). He is also with the Department of Electrical and Computer Engineering, National University of Singapore, Singapore 117583 (e-mail: elezhang@nus.edu.sg).

I. INTRODUCTION

THE past few decades have witnessed the rapid development of wireless communication technologies and the tremendous changes it has brought to our lives. In the process of wireless systems evolution from generation to generation, larger capacity and higher reliability have always been the main objectives to pursue. Multiple-input multiple-output (MIMO) or multi-user/multi-antenna communication has been a key enabling technology in this pursuit, which lifts the veil on the new degrees of freedom (DoFs) in the spatial domain for improving the communication performance [1]–[3]. By leveraging the beamforming gain and multiplexing gain, the capacity can be drastically increased with MIMO systems. Besides, the transmission reliability can be significantly improved in virtue of the spatial diversity provided by multiple antennas at the transmitter (Tx) and/or receiver (Rx). With the current trend and future expectation of wireless communication systems migrating to higher frequency bands, such as millimeter-wave and terahertz bands, the decreasing wavelength results in smaller antenna size, which renders the MIMO system to be of larger scale (a.k.a. massive MIMO) in order to compensate for the more severe propagation losses [4]–[7]. Compared to conventional MIMO, massive MIMO is able to exploit the spatial correlation of large antenna arrays for attaining higher array gains and mitigating the multi-user interference more effectively [6], [8]–[10].

However, since the antennas are deployed at fixed positions in the space, MIMO and massive MIMO cannot fully explore the spatial variation of wireless channels in a given receive area or receive field. Recently, the concept of holographic MIMO was proposed [11]–[13], which is also termed as continuous-aperture MIMO [14], holographic surface [15], or large intelligent surface [16] in the literature. The holographic MIMO is usually composed of a large number of tiny antenna elements spaced by sub-wavelength. As the element spacing approaches zero and the number of antenna elements goes infinity, the holographic MIMO can be regarded as a continuous-aperture antenna array or surface with programmable electromagnetic property. By utilizing the theory of electromagnetic information, the ultimate performance limit of communication systems subject to a given receive field can be characterized. Although the emergence of metamaterials brings new opportunities for the fabrication of holographic MIMO or holographic surface, it is still in the stage of theoretical exploration [11]–[14], [16]. Its main technical challenge lies in the high penetration loss of metamaterial-based antenna elements at the Tx and/or Rx. Besides, for holographic MIMO, the signals are controlled

by generating desired current distribution on the spatially-continuous surface. Compared to conventional discrete-aperture antennas connected with radio frequency (RF) chains, which are able to efficiently perform digital signal processing, the current distribution on holographic MIMO surfaces is difficult to be reconfigured in real time. Thus, holographic MIMO encounters fundamental limitations on processing broadband signals and still has a long journey for realizing its applications in practical systems.

Despite the above challenges, holographic MIMO has great significance on analyzing the asymptotic capacity of wireless channels and reveals the potentials of new DoFs in the continuous spatial domain for improving the communication performance [11]–[14], [16]. To exploit such spatial DoFs, we propose a new antenna architecture, namely movable antenna (MA), in this paper. Different from conventional fixed-position antennas (FPAs), the positions of MAs can be flexibly adjusted in a spatial region for improving the channel condition and enhancing the communication performance. For example, considering the spatial fading of the channels, an MA can be moved from a position with low channel gain to another position with higher channel gain. Thus, the spatial diversity can be easily obtained by adjusting the position of the MA. For MIMO systems, the positions of the multiple MAs at the Tx and Rx can be jointly designed for maximizing the channel capacity, where the positioning optimization for the MAs not only increases the channel gain of each antenna but also balances the multiplexing performance of parallel spatial data streams by properly reshaping the MIMO channel matrix.

The MA systems resemble the widely explored distributed antenna system (DAS), where the remote antenna units (RAUs) are geographically distributed in wireless networks [17]–[19]. The RAUs are connected to a single central unit (e.g., by optical fibers or coaxial cables) for centralized control and signal processing. The MA system can be implemented in a similar way where the antenna is connected to the radio-frequency (RF) chain via flexible cables. The position of the MA can be mechanically adjusted with the aid of drive components, such as stepper motors. The authors in [20] showed a prototype of MA-enabled multi-static radar, where the transmit and receive antennas are connected to the vector network analyzer via flexible armored antenna feeders and can be moved with the aid of linear drives. In [21], a reconfigurable antenna array was designed, where the array elements can move along a semicircular path with the aid of stepper motors to synthesize the radiation pattern. It is worth noting that despite the similar hardware implementation, the MA system proposed in this paper is distinguished from the DAS in terms of application scenarios and system setups. The DAS usually separates the antennas far

away from each other [17]–[19], such that the channels are independent for multiple antennas and the performance is mainly determined by the large-scale path loss of the channel. In contrast, the proposed MA system in this paper deploys the antennas in a small region with a typical size in the order of several to tens of wavelengths, which is easier to implement and has much shorter connecting cables compared to the DAS. The channels for multiple MAs experience inherent spatial correlation and thus the communication performance is dominated by the small-scale fading in the target region.

In a given receive region, if the MA can be rapidly deployed at the position with the highest channel gain, the receive signal-to-noise ratio (SNR) can be maximized, which can be regarded as a new way to acquire the spatial diversity gain. The authors in [22] proposed a novel fluid antenna system (FAS) with great flexibility in the antenna position. The fluid antenna can be freely switched to one of the candidate positions over a fixed-length line space so as to receive the strongest signal. By exploiting the selection diversity, the outage probability of the FAS can be significantly decreased compared to conventional FPA systems and may even outperform multiple-antenna systems with maximum ratio combining (MRC). In addition, a fluid antenna multiple access (FAMA) system was proposed in [23] to support transceivers with different channel conditions simultaneously. By optimizing the positions of the fluid antennas of users, the interference can be efficiently mitigated in the deep fading region and a favorable channel condition for the desired signal can be obtained, which helps improve the performance of multiple access. The research works in [22] and [23] reveal the potentials for improving the communication performance by changing the position of the antenna. However, limited by the physical characteristics, the liquid antenna can only be moved over a one-dimensional (1D) region. In contrast, the proposed MA system employs mechanical drives to move the conventional solid antenna, which can be flexibly deployed in the two-dimensional (2D) plane or three-dimensional (3D) space. Compared to FAS, the MA communication system is easier to implement and is able to fully exploit the spatial diversity/interference mitigation gains in a given field.

Moreover, the proposed MA-enabled communication system has unique advantages in comparison with the conventional antenna selection (AS) technique. To acquire high diversity order, the AS system needs to employ a large number of antenna elements [24], [25], while the MA system can exploit the full spatial diversity with much fewer or even one single antenna moving in the same region. Besides, the flexible deployment of MAs can also alleviate the interference from/to

TABLE I
COMPARISON OF MA WITH OTHER ANTENNA TECHNOLOGIES.

Technology	Movement	Number of antennas at Tx/Rx	Number of RF chains at Tx/Rx	Hardware cost	Diversity gain	Interference mitigation gain
MA	1D/2D/3D	1	1	Low	High	Medium
FAS	1D	1	1	Medium	Medium	Low
FPA	None	1	1	Very low	None	None
AS	None	N	1	Medium	Medium	Low
FPA-MIMO	None	N	N	High	High	High
MA-MIMO	1D/2D/3D	$< N$	$< N$	Medium	Very high	Very high

undesired terminals such that the interference mitigation gain is achieved for simultaneously supporting multiple transceivers. Compared to conventional MIMO systems with FPAs, the MA-enabled MIMO system can efficiently improve the channel gain and capacity. Thus, the number of required antennas and RF chains can be significantly decreased. A detailed comparison between the aforementioned technologies and MA is summarized in Table I, where N denotes the number of antennas/RF chains at the Tx or Rx in MIMO systems.

Given the above advantages of MA, we aim to investigate in this paper the channel modeling and performance analysis for MA-enabled communication systems. To characterize the general multi-path channel in a given region or field where the MAs are deployed, a field-response model is developed by leveraging the amplitude, phase, and angle of arrival/angle of departure (AoA/AoD) information on each of the multiple channel paths under the far-field condition. We show that the proposed field-response based channel model is consistent with the conventional channel models with FPAs, and present the conditions under which the field-response based channel model becomes the well-known line-of-sight (LoS) channel, geometric channel, Rayleigh and Rician fading channel models. Based on the proposed channel model, we then analyze the maximum channel gain achieved by a single receive MA as compared to its FPA counterpart in both deterministic and stochastic channels. First, in the deterministic channel case, we show the periodic behavior of the multi-path channel gain in a given spatial field, which can be exploited for analyzing the maximum channel gain of the MA. Next, in the case of stochastic channels, the expected value of an upper bound on the maximum channel gain of the MA in an infinitely large receive region is derived for different numbers of channel paths. The approximate cumulative distribution function (CDF) for the maximum channel gain is also obtained in closed form, which is useful to evaluate the outage probability of the MA system. Moreover, our results reveal that higher performance gains by the MA over the FPA can be acquired when the number of

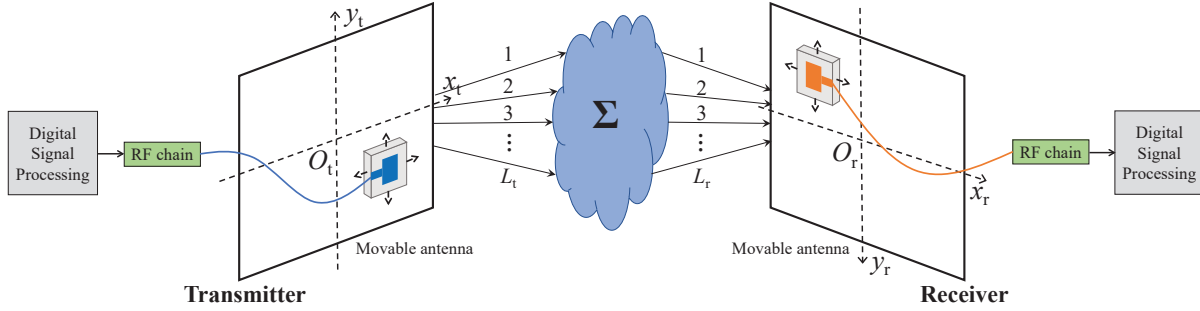


Fig. 1. Illustration of the MA-enabled communication system.

channel paths increases due to more pronounced small-scale fading effects in the spatial domain. Extensive simulations are carried out to verify our analytical results and compare the performance of the proposed MA-enabled communication system with conventional FPA systems. The results demonstrate that the MA system can reap considerable performance gains over the FPA systems with/without AS, and even achieve comparable performance to the single-input multiple-output (SIMO) beamforming system.

The rest of this paper is organized as follows. Section II introduces the signal model and the field-response based channel model for the MA-enabled communication system, where the relationship between the developed new model for MAs and the conventional channel models for FPAs is also presented. In Section III, we show the main analytical results for MA under both deterministic and stochastic channels. Simulation results are provided in Section IV and this paper is concluded in Section V.

Notation: a , \mathbf{a} , \mathbf{A} , and \mathcal{A} denote a scalar, a vector, a matrix, and a set, respectively. $(\cdot)^T$, $(\cdot)^*$, and $(\cdot)^H$ denote transpose, conjugate, and conjugate transpose, respectively. $\mathcal{CN}(\mathbf{0}, \mathbf{\Lambda})$ denotes the circularly symmetric complex Gaussian (CSCG) distribution with mean zero and covariance matrix $\mathbf{\Lambda}$. $\mathbb{E}\{\cdot\}$ denotes the expected value of a random variable. \mathbb{Z} , \mathbb{R} , and \mathbb{C} represent the sets of integers, real numbers, and complex numbers, respectively. $\Re(\cdot)$, $\Im(\cdot)$, $|\cdot|$, and $\angle(\cdot)$ denote the real part, the imaginary part, the amplitude, and the phase of a complex number or complex vector, respectively. $\text{diag}\{\mathbf{a}\}$ is a diagonal matrix with the element in row i and column i equal to the i -th element of vector \mathbf{a} . $d(\cdot)$ and $\partial(\cdot)$ denote the differential and the partial differential of a function, respectively. $\mathbf{1}_L$ denotes an L -dimensional vector with all the elements equal to 1. \mathbf{I}_L denotes an identical matrix of size $L \times L$.

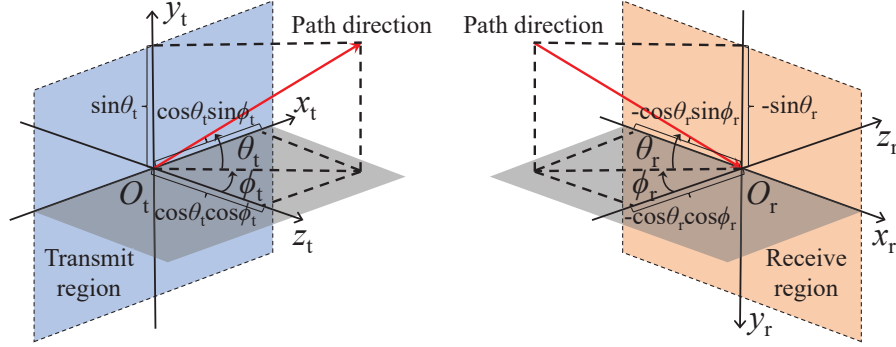


Fig. 2. Illustration of the coordinates and spatial angles for transmit and receive regions.

II. SYSTEM MODEL

The architecture of MA-enabled communication system is shown in Fig. 1, where the transmit and receive MAs are connected to the RF chains via flexible wires, such as coaxial cables. Thus, the positions of the MAs can be mechanically adjusted with the aid of drive components, such as stepper motors. The Cartesian coordinate systems, x_t - O_t - y_t and x_r - O_r - y_r , are established to describe the positions of the MAs in the transmit and receive regions, \mathcal{C}_t and \mathcal{C}_r , respectively¹. The coordinates of the transmit MA are denoted as $\mathbf{t} = [x_t, y_t]^T$, and the coordinates of the receive MA are denoted as $\mathbf{r} = [x_r, y_r]^T$.

For the considered MA system, the channel response depends on the positions of the antennas. Thus, the channel coefficient can be represented by a function of the positions of the transmit and receive MAs, i.e., $h(\mathbf{t}, \mathbf{r})$. Denoting the transmit power of the Tx as p_t , the received signal at the Rx can be expressed as

$$y(\mathbf{t}, \mathbf{r}) = h(\mathbf{t}, \mathbf{r})\sqrt{p_t}s + n, \quad \mathbf{t} \in \mathcal{C}_t, \mathbf{r} \in \mathcal{C}_r, \quad (1)$$

where s represents the transmit signal with zero mean and normalized power of one, and $n \sim \mathcal{CN}(0, \delta^2)$ is the white Gaussian noise at the Rx with power δ^2 . As a result, the SNR for the received signal is given by

$$\gamma(\mathbf{t}, \mathbf{r}) = \frac{|h(\mathbf{t}, \mathbf{r})|^2 p_t}{\delta^2}, \quad \mathbf{t} \in \mathcal{C}_t, \mathbf{r} \in \mathcal{C}_r. \quad (2)$$

¹In this paper, we consider the MAs moving in a 2D plane, which can be extended to the 3D space by adding the $z_t(z_r)$ coordinate.

A. Field-Response Based Channel Model

For MA systems, the channel response is determined by the propagation environments and the positions of the antennas. In this paper, we assume that the size of the region for moving the antenna is much smaller than the propagation distance between the Tx and Rx, such that the far-field condition is satisfied at the Tx and Rx. This assumption is reasonable because the typical size of the antenna moving region is in the order of several to tens of wavelengths. For example, for an MA system operating at 28 GHz, the area of a square region with ten-wavelength sides is approximate 0.01 m^2 , for which the far-field condition can be easily guaranteed in this region. Thus, the plane-wave model can be used to form the field response between the transmit and receive regions. In other words, the AoDs, AoAs, and amplitudes of complex coefficients for the multiple channel paths do not change for different positions of the MAs, while only the phases of the multi-path channels vary in the transmit/receive region.

At the Tx side, we denote the number of transmit paths as L_t . As shown in Fig. 2, the elevation and azimuth AoDs of the j -th transmit path are respectively denoted as $\theta_{t,j} \in [-\pi/2, \pi/2]$ and $\phi_{t,j} \in [-\pi/2, \pi/2]$, $1 \leq j \leq L_t$. At the Rx side, we denote the number of receive paths as L_r . The elevation and azimuth AoAs of the i -th receive path are respectively denoted as $\theta_{r,i} \in [-\pi/2, \pi/2]$ and $\phi_{r,i} \in [-\pi/2, \pi/2]$, $1 \leq i \leq L_r$. We define a path-response matrix (PRM) $\Sigma \in \mathbb{C}^{L_r \times L_t}$ to represent the response from the transmit reference position $\mathbf{t}_0 = (0, 0)$ to the receive reference position $\mathbf{r}_0 = (0, 0)$. Specifically, the entry in row i and column j of Σ , denoted as $\sigma_{i,j}$, is the response coefficient between the j -th transmit path and the i -th receive path. As a result, the channel between two antennas located at \mathbf{t}_0 and \mathbf{r}_0 is given by

$$h(\mathbf{t}_0, \mathbf{r}_0) = \mathbf{1}_{L_r}^H \Sigma \mathbf{1}_{L_t}, \quad (3)$$

which is the linear superposition of all the elements in the PRM.

According to basic geometry shown in Fig. 2, the difference of the signal propagation distance between position $\mathbf{r} = [x_r, y_r]$ and the reference point \mathbf{r}_0 is given by $\rho_{r,i}(x_r, y_r) = x_r \cos \theta_{r,i} \sin \phi_{r,i} + y_r \sin \theta_{r,i}$ for the i -th receive path, $1 \leq i \leq L_r$. It indicates that the channel response of the i -th receive path at position \mathbf{r} has a $2\pi\rho_{r,i}(x_r, y_r)/\lambda$ phase difference with respect to the reference point \mathbf{r}_0 , where λ is the wavelength. To account for such phase differences in all L_r receive paths, the field-response vector (FRV) in the receive region is defined as

$$\mathbf{f}(\mathbf{r}) = [e^{j\frac{2\pi}{\lambda}\rho_{r,1}(x_r, y_r)}, e^{j\frac{2\pi}{\lambda}\rho_{r,2}(x_r, y_r)}, \dots, e^{j\frac{2\pi}{\lambda}\rho_{r,L_r}(x_r, y_r)}]^T. \quad (4)$$

Similarly, for any position $\mathbf{t} = [x_t, y_t]$ in the transmit region, the FRV is defined as

$$\mathbf{g}(\mathbf{t}) = [e^{j\frac{2\pi}{\lambda}\rho_{t,1}(x_t,y_t)}, e^{j\frac{2\pi}{\lambda}\rho_{t,2}(x_t,y_t)}, \dots, e^{j\frac{2\pi}{\lambda}\rho_{t,L_t}(x_t,y_t)}]^T. \quad (5)$$

with $\rho_{t,j}(x_t, y_t) = x_t \cos \theta_{t,j} \sin \phi_{t,j} + y_t \sin \theta_{t,j}$, $1 \leq j \leq L_t$. As a result, the channel between two antennas located at positions $\mathbf{t} = [x_t, y_t]$ and $\mathbf{r} = [x_r, y_r]$ is obtained as

$$h(\mathbf{t}, \mathbf{r}) = \mathbf{f}(\mathbf{r})^H \mathbf{\Sigma} \mathbf{g}(\mathbf{t}). \quad (6)$$

B. Relationship with Conventional Channel Models

The channel model shown in (6) characterizes the wireless channel based on the transmit/receive antenna locations to facilitate our subsequent performance analysis for MA-enabled communications. For any given positions of the transmit and receive MAs, the channel model in (6) is consistent with that of the conventional FPA systems. In this subsection, we present the conditions under which the model in (6) becomes the well-known LoS channel, geometric channel, Rayleigh and Rician fading channels.

1) *LoS Channel*: A necessary condition for (6) being equivalent to the LoS channel is that the numbers of transmit and receive paths are both equal to 1, i.e.,

$$L_t = L_r = 1. \quad (7)$$

Under this condition, the PRM and FRVs are all reduced to scalars, i.e.,

$$\begin{cases} \mathbf{\Sigma} = \sigma_{1,1}, \\ \mathbf{f}(\mathbf{r}) = e^{j\frac{2\pi}{\lambda}(x_r \cos \theta_{r,1} \sin \phi_{r,1} + y_r \sin \theta_{r,1})}, \\ \mathbf{g}(\mathbf{t}) = e^{j\frac{2\pi}{\lambda}(x_t \cos \theta_{t,1} \sin \phi_{t,1} + y_t \sin \theta_{t,1})}, \end{cases} \quad (8)$$

where $\sigma_{1,1}$, $\theta_{r,1}$, $\phi_{r,1}$, $\theta_{t,1}$, and $\phi_{t,1}$ represent the path-response coefficient at antenna positions $(\mathbf{t}_0, \mathbf{r}_0)$, the elevation AoA, azimuth AoA, elevation AoD, and azimuth AoD for the LoS path, respectively.

2) *Geometric Channel*: For geometric channels, the transmit and receive paths have one-to-one correspondence. In other words, each transmit path always arrives at the Rx through one and only one receive path. Thus, a necessary condition for (6) to be the geometric channel is given by

$$L_t = L_r = L. \quad (9)$$

Under this condition, the PRM becomes diagonal, i.e.,

$$\Sigma = \text{diag}\{\sigma_{1,1}, \sigma_{2,2}, \dots, \sigma_{L,L}\}, \quad (10)$$

where $\sigma_{i,i}$, $1 \leq i \leq L$, represents the path-response coefficient corresponding to antenna positions $(\mathbf{t}_0, \mathbf{r}_0)$ for the i -th path component between the Tx and Rx.

3) *Rayleigh Fading Channel*: A necessary condition for (6) to represent Rayleigh fading is that infinite number of statistically independent paths exist between the transmit and receive regions. Thus, the numbers of transmit and receive paths should approach infinity, i.e.,

$$L_t \rightarrow +\infty, \quad L_r \rightarrow +\infty. \quad (11)$$

Besides, for isotropic scattering environments, the multi-path components should be uniformly distributed over the half-space in front of the antenna panel, which yields the AoDs and AoAs following the probability density functions (PDFs)

$$f_{\text{AoD}}(\theta_t, \phi_t) = \frac{\cos \theta_t}{2\pi}, \quad \theta_t \in \left[-\frac{\pi}{2}, \frac{\pi}{2}\right], \quad \phi_t \in \left[-\frac{\pi}{2}, \frac{\pi}{2}\right], \quad (12a)$$

$$f_{\text{AoA}}(\theta_r, \phi_r) = \frac{\cos \theta_r}{2\pi}, \quad \theta_r \in \left[-\frac{\pi}{2}, \frac{\pi}{2}\right], \quad \phi_r \in \left[-\frac{\pi}{2}, \frac{\pi}{2}\right], \quad (12b)$$

respectively. Under the above conditions, if the elements of the PRM are independent and identically distributed (i.i.d.) circularly symmetric complex random variables, according to the central limit theory, the superimposed path responses at the Tx and Rx, i.e., the elements of $\mathbf{f}(\mathbf{r})^H \Sigma$ and $\Sigma \mathbf{g}(\mathbf{t})$, are i.i.d. CSCG distributed random variables. Thus, the channel coefficient $h(\mathbf{t}, \mathbf{r}) = \mathbf{f}(\mathbf{r})^H \Sigma \mathbf{g}(\mathbf{t})$, which is equal to the sum of all the elements of $\mathbf{f}(\mathbf{r})^H \Sigma$ weighted by the unit-modulus elements of $\mathbf{g}(\mathbf{t})$, or the sum of all the elements of $\Sigma \mathbf{g}(\mathbf{t})$ weighted by the unit-modulus elements of $\mathbf{f}(\mathbf{r})^H$, is also a CSCG random variable, which leads to Rayleigh fading.

4) *Rician Fading Channel*: For Rician fading, an LoS path exists between the Tx and the Rx, and the NLoS components are also uniformly distributed over the half-space similar to that of the Rayleigh fading. Thus, the numbers of transmit and receive paths should approach infinity as shown in (11), and the elements of the PRM are i.i.d. circularly symmetric complex random variables. Meanwhile, the element in row i^* and column j^* of Σ corresponding to the LoS path

has a constant amplitude. The Rician factor is thus obtained as

$$\kappa = \frac{|\sigma_{i^*,j^*}|^2}{\mathbb{E} \left\{ \left| \sum_{(i,j) \neq (i^*,j^*)} \sigma_{i,j} \right|^2 \right\}}. \quad (13)$$

III. PERFORMANCE ANALYSIS

To analyze the performance gain provided by MAs over conventional FPAs, we consider the simplified scenario where the position of the transmit antenna is fixed at the reference point \mathbf{t}_0 while the position of the receive antenna can be flexible. Thus, the signal model can be simplified as

$$y(\mathbf{r}) = \mathbf{f}(\mathbf{r})^H \Sigma \mathbf{g}(\mathbf{t}_0) \sqrt{p_t} s + n \triangleq \mathbf{f}(\mathbf{r})^H \mathbf{b} \sqrt{p_t} s + n, \quad \mathbf{r} \in \mathcal{C}_r, \quad (14)$$

where $\mathbf{b} = \Sigma \mathbf{g}(\mathbf{t}_0) \triangleq [b_1, b_2, \dots, b_{L_r}]^T$ represents the effective path-response vector (EPRV) in the receive region. Since the channel gain varies with the position of the receive MA, the receive SNR in (2) changes accordingly. In this section, the maximum channel gain achievable by a single receive MA and the corresponding SNR gain over an FPA located at \mathbf{r}_0 are analyzed under the deterministic and stochastic channel setups, respectively.

A. Deterministic Channel

In this subsection, we analyze the characteristics of the channel gain in the receive region for deterministic path responses with any given EPRV \mathbf{b} and physical AoAs $\theta_{r,\ell}$ and $\phi_{r,\ell}$, $1 \leq \ell \leq L_r$. For notation simplicity, we define intermediate variables $\varphi_{r,\ell} = \cos \theta_{r,\ell} \sin \phi_{r,\ell}$ and $\vartheta_{r,\ell} = \sin \theta_{r,\ell}$ as the virtual AoAs for the ℓ -th receive path, $1 \leq \ell \leq L_r$. Then, the property of the channel gain can be analyzed separately for the one-path, two-path, three-path, and multiple-path cases as follows.

1) *One-Path Case:* If only one channel path arrives at the Rx, the channel (power) gain is a constant within the receive region, i.e.,

$$|h_1(\mathbf{r})|^2 = |e^{-j2\pi(\frac{z_r}{\lambda} \varphi_{r,1} + \frac{y_r}{\lambda} \vartheta_{r,1})} b_1|^2 = |b_1|^2. \quad (15)$$

In other words, the change of the antenna position can only impact the phase of the channel for the one-path case and the MA cannot provide any SNR gain over the FPA.

2) *Two-Path Case*: If two channel paths with different AoAs arrive at the Rx, the channel gain between the transmit antenna and the receive MA at position \mathbf{r} is given by

$$\begin{aligned} |h_2(\mathbf{r})|^2 &= |e^{-j2\pi(\frac{x_r}{\lambda}\varphi_{r,1} + \frac{y_r}{\lambda}\vartheta_{r,1})}b_1 + e^{-j2\pi(\frac{x_r}{\lambda}\varphi_{r,2} + \frac{y_r}{\lambda}\vartheta_{r,2})}b_2|^2 \\ &= |b_1|^2 + |b_2|^2 + 2\Re \left\{ b_1^* b_2 e^{j2\pi\left[\left(\frac{x_r}{\lambda}\varphi_{r,1} + \frac{y_r}{\lambda}\vartheta_{r,1}\right) - \left(\frac{x_r}{\lambda}\varphi_{r,2} + \frac{y_r}{\lambda}\vartheta_{r,2}\right)\right]} \right\} \\ &= |b_1|^2 + |b_2|^2 + 2|b_1||b_2| \cos \{ \omega_{1,2}(x_r, y_r) \}, \end{aligned} \quad (16)$$

with intermediate variables $\omega_{1,2}(x_r, y_r) = 2\pi \left[\frac{x_r}{\lambda}(\varphi_{r,1} - \varphi_{r,2}) + \frac{y_r}{\lambda}(\vartheta_{r,1} - \vartheta_{r,2}) \right] + \mu_2 - \mu_1$ and parameters $\mu_\ell = \angle b_\ell$, $\ell = 1, 2$. As can be observed, the superimposed power of the two paths has a periodic character in the receive region due to the existence of the cosine function. For any fixed y_r , the period of the channel gain along axis x_r is given by $\lambda/(\varphi_{r,1} - \varphi_{r,2})$. It indicates that a larger difference of the virtual AoAs $\varphi_{r,1}$ and $\varphi_{r,2}$ yields a smaller period along axis x_r . Similarly, for any fixed x_r , the period of the channel gain along axis y_r is given by $\lambda/(\vartheta_{r,1} - \vartheta_{r,2})$.

To analyze the variation of the channel gain in the receive region, the gradient of the channel gain with respect to the MA position can be derived as

$$\nabla |h_2(\mathbf{r})|^2 = \left[\frac{\partial |h_2(\mathbf{r})|^2}{\partial x_r}, \frac{\partial |h_2(\mathbf{r})|^2}{\partial y_r} \right]^T = [g_{x_r, y_r} \times (\varphi_{r,1} - \varphi_{r,2}), g_{x_r, y_r} \times (\vartheta_{r,1} - \vartheta_{r,2})]^T, \quad (17)$$

with $g_{x_r, y_r} = -\frac{4\pi}{\lambda}|b_1||b_2| \sin \{ 2\pi \left[\frac{x_r}{\lambda}(\varphi_{r,1} - \varphi_{r,2}) + \frac{y_r}{\lambda}(\vartheta_{r,1} - \vartheta_{r,2}) \right] + \mu_2 - \mu_1 \}$. Thus, for any position excluding the maximum points, the direction for increasing the channel gain most quickly is given by $[(\varphi_{r,1} - \varphi_{r,2}), (\vartheta_{r,1} - \vartheta_{r,2})]^T$ or $[(\varphi_{r,2} - \varphi_{r,1}), (\vartheta_{r,2} - \vartheta_{r,1})]^T$. The MA can be moved along the gradient direction for approaching the maximum channel gain in the receive region most efficiently. Moreover, it can be easily derived that a tight upper bound on the maximum channel gain is

$$\max_{\mathbf{r} \in \mathcal{C}_r} |h_2(\mathbf{r})|^2 = (|b_1| + |b_2|)^2, \quad (18)$$

which can be achieved at positions satisfying

$$2\pi \left[\frac{x_r}{\lambda}(\varphi_{r,1} - \varphi_{r,2}) + \frac{y_r}{\lambda}(\vartheta_{r,1} - \vartheta_{r,2}) \right] + \mu_2 - \mu_1 = 2k\pi, \quad k \in \mathbb{Z}. \quad (19)$$

The equation in (19) yields parallel lines in the x_r - y_r plane. An example for the channel gain with two receive paths is shown in Fig. 3, where the distance of any two adjacent maximum

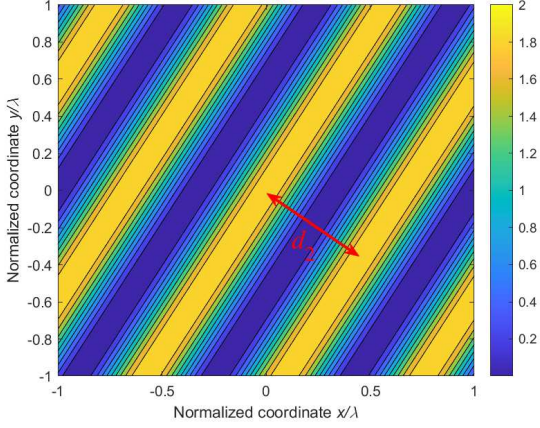


Fig. 3. Illustration of the periodic character of the channel gain in the receive region, with $L_r = 2$, $b_1 = b_2 = \frac{\sqrt{2}}{2}$, $\theta_{r,1} = 0$, $\theta_{r,2} = \frac{\pi}{3}$, $\phi_{r,1} = \frac{\pi}{2}$, and $\phi_{r,2} = -\frac{\pi}{2}$.

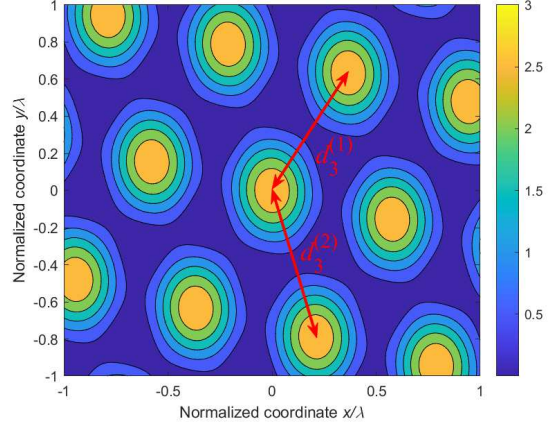


Fig. 4. Illustration of the periodic character of the channel gain in the receive region, with $L_r = 3$, $b_1 = b_2 = b_3 = \frac{\sqrt{3}}{3}$, $\theta_{r,1} = 0$, $\theta_{r,2} = \frac{\pi}{3}$, $\theta_{r,3} = -\frac{\pi}{4}$, $\phi_{r,1} = \frac{\pi}{2}$, $\theta_{r,2} = -\frac{\pi}{2}$, and $\theta_{r,3} = -\frac{\pi}{2}$.

lines can be obtained as

$$d_2 = \frac{\lambda}{\sqrt{(\varphi_{r,1} - \varphi_{r,2})^2 + (\vartheta_{r,1} - \vartheta_{r,2})^2}}. \quad (20)$$

According to basic geometry, the upper bound on the channel gain can always be achieved if the receive region is a circular area with diameter larger than d_2 . Thus, we know that to achieve the upper bound on the channel gain, a smaller area of the region is required if the AoA difference of the two paths is larger.

3) *Three-Path Case*: If the number of receive paths is three, the channel gain between the transmit antenna and the receive MA at position \mathbf{r} is given by

$$\begin{aligned} |h_3(\mathbf{r})|^2 &= |e^{-j2\pi(\frac{x_r}{\lambda}\varphi_{r,1} + \frac{y_r}{\lambda}\vartheta_{r,1})}b_1 + e^{-j2\pi(\frac{x_r}{\lambda}\varphi_{r,2} + \frac{y_r}{\lambda}\vartheta_{r,2})}b_2 + e^{-j2\pi(\frac{x_r}{\lambda}\varphi_{r,3} + \frac{y_r}{\lambda}\vartheta_{r,3})}b_3|^2 \\ &= |b_1|^2 + |b_2|^2 + |b_3|^2 + 2|b_1||b_2|\cos\{\omega_{1,2}(x_r, y_r)\} \\ &\quad + 2|b_1||b_3|\cos\{\omega_{1,3}(x_r, y_r)\} + 2|b_2||b_3|\cos\{\omega_{2,3}(x_r, y_r)\}, \end{aligned} \quad (21)$$

with intermediate variables $\omega_{m,n}(x_r, y_r) = 2\pi \left[\frac{x_r}{\lambda}(\varphi_{r,m} - \varphi_{r,n}) + \frac{y_r}{\lambda}(\vartheta_{r,m} - \vartheta_{r,n}) \right] + \mu_n - \mu_m$, $1 \leq m < n \leq 3$, and parameters $\mu_\ell = \angle b_\ell$, $\ell = 1, 2, 3$. It can be observed that the channel gain in (21) also has a periodic character. Specifically, let $\mathbf{r}_p = [x_p, y_p]^T$ denote the period vector for the channel gain, i.e., we have $|h_3(\mathbf{r})|^2 \equiv |h_3(\mathbf{r} + \mathbf{r}_p)|^2$ for any $\mathbf{r}, \mathbf{r} + \mathbf{r}_p \in \mathcal{C}_r$. A sufficient condition for \mathbf{r}_p being the period of the channel gain is given by

$$\cos\{\omega_{m,n}(x_r, y_r)\} \equiv \cos\{\omega_{m,n}(x_r + x_p, y_r + y_p)\}, \quad 1 \leq m < n \leq 3, \quad (22)$$

for $\forall [x_r, y_r]^T, [x_r + x_p, y_r + y_p]^T \in \mathcal{C}_r$, which can be equivalently converted to

$$\frac{x_p}{\lambda}(\varphi_{r,m} - \varphi_{r,n}) + \frac{y_p}{\lambda}(\vartheta_{p,m} - \vartheta_{p,n}) = k_{m,n} \in \mathbb{Z}, \quad 1 \leq m < n \leq 3. \quad (23)$$

The solution for (23) can be obtained by directly solving the equation set as

$$\begin{cases} x_p = \frac{\lambda}{\xi_1} [k_{1,2} (\vartheta_{r,1} - \vartheta_{r,3}) - k_{1,3} (\vartheta_{r,1} - \vartheta_{r,2})], \\ y_p = \frac{\lambda}{\xi_2} [k_{1,2} (\varphi_{r,1} - \varphi_{r,3}) - k_{1,3} (\varphi_{r,1} - \varphi_{r,2})], \end{cases} \quad (24)$$

with $\xi_1 = (\varphi_{r,1} - \varphi_{r,2})(\vartheta_{r,1} - \vartheta_{r,3}) - (\varphi_{r,1} - \varphi_{r,3})(\vartheta_{r,1} - \vartheta_{r,2})$, $\xi_2 = (\vartheta_{r,1} - \vartheta_{r,2})(\varphi_{r,1} - \varphi_{r,3}) - (\vartheta_{r,1} - \vartheta_{r,3})(\varphi_{r,1} - \varphi_{r,2})$, $k_{1,2}, k_{1,3} \in \mathbb{Z}$, and $k_{2,3} = k_{1,3} - k_{1,2}$.

If the arguments in (22) are all equal to their maximum value, i.e., one, a tight upper bound on the maximum channel gain can be obtained as

$$\max_{\mathbf{r} \in \mathcal{C}_r} |h_3(\mathbf{r})|^2 = (|b_1| + |b_2| + |b_3|)^2, \quad (25)$$

which can be achieved at positions satisfying

$$2\pi \left[\frac{x_r}{\lambda}(\varphi_{r,1} - \varphi_{r,2}) + \frac{y_r}{\lambda}(\vartheta_{r,1} - \vartheta_{r,2}) \right] + \mu_2 - \mu_1 = 2k_1\pi, \quad k_1 \in \mathbb{Z} \quad (26a)$$

$$2\pi \left[\frac{x_r}{\lambda}(\varphi_{r,1} - \varphi_{r,3}) + \frac{y_r}{\lambda}(\vartheta_{r,1} - \vartheta_{r,3}) \right] + \mu_3 - \mu_1 = 2k_2\pi, \quad k_2 \in \mathbb{Z} \quad (26b)$$

$$2\pi \left[\frac{x_r}{\lambda}(\varphi_{r,2} - \varphi_{r,3}) + \frac{y_r}{\lambda}(\vartheta_{r,2} - \vartheta_{r,3}) \right] + \mu_3 - \mu_2 = 2k_3\pi, \quad k_3 \in \mathbb{Z}. \quad (26c)$$

It can be verified that constraint (26c) can be safely removed because it holds if and only if constraints (26a), (26b), and $k_3 = k_2 - k_1$ are satisfied. Thus, the tight upper bound on the maximum channel gain is achieved at the intersections of the lines determined by (26a) and (26b), with the coordinates accordingly given by

$$\begin{cases} x_r^* = \frac{\lambda}{2\pi\xi_1} [(2k_1\pi + \mu_1 - \mu_2)(\vartheta_{r,1} - \vartheta_{r,3}) - (2k_2\pi + \mu_1 - \mu_3)(\vartheta_{r,1} - \vartheta_{r,2})], \\ y_r^* = \frac{\lambda}{2\pi\xi_2} [(2k_1\pi + \mu_1 - \mu_2)(\varphi_{r,1} - \varphi_{r,3}) - (2k_2\pi + \mu_1 - \mu_3)(\varphi_{r,1} - \varphi_{r,2})], \end{cases} \quad (27)$$

for $\forall k_1, k_2 \in \mathbb{Z}$. An example for the the channel gain with three receive paths is provided in

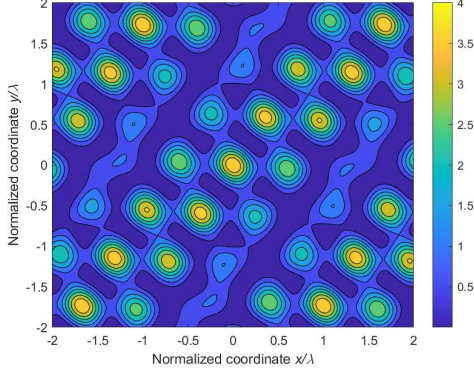


Fig. 5. An example for the channel gain in the receive region, with $L_r = 4$, $b_1 = b_2 = b_3 = b_4 = \frac{1}{2}$, $\theta_{r,1} = 0$, $\theta_{r,2} = \frac{\pi}{3}$, $\theta_{r,3} = -\frac{\pi}{4}$, $\theta_{r,4} = -\frac{2\pi}{3}$, $\phi_{r,1} = \frac{\pi}{2}$, $\theta_{r,2} = -\frac{\pi}{2}$, $\theta_{r,3} = -\frac{\pi}{2}$, and $\theta_{r,4} = \frac{\pi}{2}$.

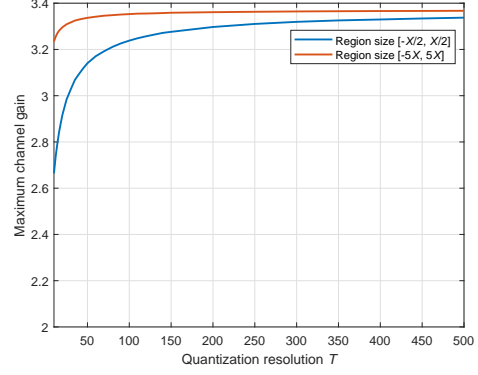


Fig. 6. Performance comparison for the maximum channel gains with varying angle quantization resolution, where the number of receive paths is $L_r = 4$ and the vertical axis is fixed at $y_r = 0$.

Fig. 4, where the distance of any two adjacent maximum points can be obtained as

$$\begin{cases} d_3^{(1)} = \lambda \sqrt{\left(\frac{\vartheta_{r,1} - \vartheta_{r,2}}{\xi_1}\right)^2 + \left(\frac{\varphi_{r,1} - \varphi_{r,2}}{\xi_2}\right)^2}, \\ d_3^{(2)} = \lambda \sqrt{\left(\frac{\vartheta_{r,1} - \vartheta_{r,3}}{\xi_1}\right)^2 + \left(\frac{\varphi_{r,1} - \varphi_{r,3}}{\xi_2}\right)^2}. \end{cases} \quad (28)$$

According to basic geometry, the upper bound on the channel gain can always be achieved if the receive region is a circular area with diameter larger than $d_3 = \sqrt{\left(d_3^{(1)}\right)^2 + \left(d_3^{(2)}\right)^2}$.

4) *Multiple-Path Case*: If the number of receive paths is larger than three, the channel gain between the transmit antenna and the receive MA at position \mathbf{r} is given by

$$|h_{L_r}(\mathbf{r})|^2 = \left| \sum_{\ell=1}^{L_r} b_\ell e^{-j2\pi\left(\frac{x_r}{\lambda}\varphi_{r,\ell} + \frac{y_r}{\lambda}\vartheta_{r,\ell}\right)} \right|^2, \quad (29)$$

which has a form similar to the 2D discrete-time Fourier transform (DTFT)². Specifically, the virtual AoAs in the angular domain can be regarded as time domain, while the positions in the spatial domain can be thought as frequency domain.

In general, the period of the channel gain cannot be obtained explicitly for $L_r > 3$ as the virtual AoAs $\varphi_{r,\ell}$ and $\vartheta_{r,\ell}$ are randomly distributed, which can be observed from Fig. 5. Nevertheless, the approximate period for the channel gain can be derived by assuming quantized AoAs. Next, we analyze the periodic character for the channel gain along axis x_r , while the periodic character

²Note that (29) holds for arbitrary values of $L_r \geq 1$.

along axis y_r can be derived in a similar way. Specifically, for any fixed y_r , we denote the channel gain between the transmit antenna and the receive MA at location (x_r, y_0) as

$$G(x_r) = |h_{L_r}(\mathbf{r})|_{y_r=y_0}^2 = \left| \sum_{\ell=1}^{L_r} b_\ell e^{-j2\pi\left(\frac{x_r}{\lambda}\varphi_{r,\ell} + \frac{y_0}{\lambda}\vartheta_{r,\ell}\right)} \right|^2 \triangleq \left| \sum_{\ell=1}^{L_r} \tilde{b}_\ell e^{-j2\pi\frac{x_r}{\lambda}\varphi_{r,\ell}} \right|^2, \quad (30)$$

with $\tilde{b}_\ell = b_\ell e^{-j2\pi\frac{y_0}{\lambda}\vartheta_{r,\ell}}$. Let X denote the period for the channel gain along axis x_r . Then, we have

$$\begin{aligned} G(x_r) &\equiv G(x_r + X) \\ &\Leftrightarrow \left| \sum_{\ell=1}^{L_r} \tilde{b}_\ell e^{-j2\pi\frac{x_r}{\lambda}\varphi_{r,\ell}} \right|^2 \equiv \left| \sum_{\ell=1}^{L_r} \tilde{b}_\ell e^{-j2\pi\frac{x_r+X}{\lambda}\varphi_{r,\ell}} \right|^2 \\ &\Leftrightarrow \sum_{m=1}^{L_r} \sum_{n=1}^{L_r} \tilde{b}_m^* \tilde{b}_n e^{j2\pi\frac{x_r}{\lambda}(\varphi_{r,m}-\varphi_{r,n})} \equiv \sum_{m=1}^{L_r} \sum_{n=1}^{L_r} \tilde{b}_m^* \tilde{b}_n e^{j2\pi\frac{x_r+X}{\lambda}(\varphi_{r,m}-\varphi_{r,n})} \\ &\Leftrightarrow \sum_{m=1}^{L_r} \sum_{n=1, n \neq m}^{L_r} \tilde{b}_m^* \tilde{b}_n \left[1 - e^{-j2\pi\frac{X}{\lambda}(\varphi_{r,m}-\varphi_{r,n})} \right] e^{-j2\pi\frac{x_r}{\lambda}(\varphi_{r,m}-\varphi_{r,n})} \equiv 0 \\ &\Leftrightarrow 1 - e^{-j2\pi\frac{X}{\lambda}(\varphi_{r,m}-\varphi_{r,n})} = 0, \quad 1 \leq m, n \leq L_r \\ &\Leftrightarrow \frac{X}{\lambda} (\varphi_{r,m} - \varphi_{r,n}) \in \mathbb{Z}, \quad 1 \leq m, n \leq L_r, \end{aligned} \quad (31)$$

which indicates that period X is the minimum real number that ensures $\frac{X}{\lambda} (\varphi_{r,m} - \varphi_{r,n})$ to be an integer for $1 \leq m, n \leq L_r$. To facilitate performance analysis, we quantize the virtual AoAs with a resolution of T , i.e., assuming $\varphi_{r,\ell} \in \{\Delta_t = -1 + \frac{2t-1}{T}\}_{1 \leq t \leq T}$. Without loss of generality, we assume that the virtual AoAs are sorted in a non-decreasing order, i.e., $\varphi_{r,1} \leq \varphi_{r,2} \leq \dots \leq \varphi_{r,L_r}$. Besides, we denote the virtual AoAs as $\varphi_{r,\ell} = \Delta_{t_\ell} = -1 + \frac{2t_\ell-1}{T}$, which means that $\varphi_{r,\ell}$ corresponds to the t_ℓ -th element in the quantized set of the virtual AoAs. Then, the difference of two adjacent virtual AoAs can be obtained as $\varphi_{r,\ell+1} - \varphi_{r,\ell} = \Delta_{t_{\ell+1}} - \Delta_{t_\ell} = \frac{2}{T}(t_{\ell+1} - t_\ell) \triangleq \frac{2\tau_\ell}{T}$, $1 \leq \ell \leq L_r$. Denote τ^* as the maximal common factor for $\{\tau_\ell\}_{1 \leq \ell \leq L_r}$. To guarantee $\frac{X}{\lambda} (\varphi_{r,m} - \varphi_{r,n})$ being integers, the period for the channel gain along axis x_r should be given by

$$X = \frac{T\lambda}{2\tau^*}. \quad (32)$$

Thus, we know that for any fixed y_r , the maximum channel gain can always be achieved if the size of the region along axis x_r is no less than period X . As can be observed from (32), the accuracy of the period is influenced by the quantization resolution T because an approximation on the AoAs is employed. If a small resolution T is used, the difference between the practical

AoAs and the approximately quantized AoAs is large, and thus the obtained period becomes inaccurate. In contrast, if a large resolution T is utilized, the obtained period is accurate because the difference between the practical AoAs and the approximately quantized AoAs is small. To evaluate the impact of the quantization resolution, we compare the maximum channel gain for different sizes of the receive region along axis x_r . Specifically, the number of receive paths is $L_r = 4$, where the virtual AoA $\varphi_{r,\ell}$ is randomly generated following uniform distribution over $[-1, 1]$. The complex path-response coefficient b_ℓ follows i.i.d. CSCG distribution with mean zero and variance $1/L_r$. For each channel realization, we obtain period X according to (32). Then, the maximum channel gains within regions $x_r \in [-X/2, X/2]$ and $x_r \in [-5X, 5X]$ are separately calculated via exhaustive search. Each point in Fig. 6 is an average result over 10^4 channel realizations. As can be observed, with the increasing quantization resolution, the performance gap between the two sizes of the region becomes smaller, which indicates that the approximation of the quantized AoAs has less impact on the maximum value of the channel gain. In other words, a higher quantization resolution can guarantee that the maximum channel gain is more likely achieved within period X .

B. Stochastic Channel

Next, we focus on the stochastic performance of the MA system. We assume that the EPRV is a CSCG random vector with i.i.d. elements, i.e., $b_\ell \sim \mathcal{CN}(0, \sigma^2/L_r)$, $1 \leq \ell \leq L_r$. Besides, the physical AoAs are assumed to be i.i.d. random variables with the PDF given in (12b). Thus, we can obtain the expected channel gain at the reference point $\mathbf{r}_0 = (0, 0)$ as

$$G_0 = \mathbb{E}\{|h(\mathbf{r}_0)|^2\} = \mathbb{E}\left\{\left|\sum_{\ell=1}^{L_r} b_\ell\right|^2\right\} = \sigma^2. \quad (33)$$

Note that since we assume far-field scenarios, the expected channel gain at any point in the receive region is equal to that at the reference point, i.e., $G(\mathbf{r}) = \left|\sum_{\ell=1}^{L_r} e^{-j2\pi(\frac{x_r}{\lambda}\varphi_{r,\ell} + \frac{y_r}{\lambda}\vartheta_{r,\ell})} b_\ell\right|^2 = \sigma^2$. This equation holds because b_ℓ is a circularly symmetric random variable for $1 \leq \ell \leq L_r$. For the FPA system, the position of the antenna should be fixed at a specific position, and thus the expected channel gain is always equal to σ^2 . In contrast, for the MA system, we can always find a position which achieves a larger channel gain in the receive region, and thus an increase on the average channel gain can be acquired over the FPA system.

1) *Single-Path Case:* As we have analyzed in Section III-A, the channel gain is a constant within the receive region if only one channel path arrives at the Rx. Thus, the maximum channel gain of the MA has an expected value equal to the expected channel gain at the reference point, i.e.,

$$G_{\max,1} = G_0 = \sigma^2, \quad (34)$$

which indicates that no SNR gain is acquired by the MA over the FPA. Furthermore, the CDF of the channel gain for the one-path case can be derived as

$$F_1(t) \triangleq \Pr \{|b_1|^2 \leq t\} = \int_0^{\sqrt{t}} \frac{2x}{\sigma^2} e^{-\frac{x^2}{\sigma^2}} dx = 1 - e^{-\frac{t}{\sigma^2}}, \quad t \geq 0. \quad (35)$$

For any given transmit power p_t , noise power δ^2 , and receive SNR threshold γ_{th} , the outage probability for the MA system with a single receive path is given by $F_1\left(\frac{\delta^2 \gamma_{\text{th}}}{p_t}\right)$.

2) *Two-Path Case:* According to Section III-A, for any given $\varphi_{r,1}, \varphi_{r,2}, \vartheta_{r,1}, \vartheta_{r,2}$, the maximum channel gain $(|b_1| + |b_2|)^2$ can always be achieved if the diameter of the receive region is larger than d_2 shown in (20). Since b_ℓ is a CSCG random variable with mean zero and variance σ^2/L_r , $|b_\ell|$ is a Rayleigh-distributed random variable with the PDF given by

$$f_{|b_\ell|}(t) = \frac{4t}{\sigma^2} e^{-\frac{2t}{\sigma^2}}, \quad t \geq 0, \quad \ell = 1, 2, \quad (36)$$

Thus, as the size of the receive region approaches infinity, the upper bound on the maximum channel gain can always be achieved for arbitrary AoAs. The expected value of the maximum channel gain of the MA in the receive region is thus given by

$$\begin{aligned} G_{\max,2} &= \mathbb{E} \{(|b_1| + |b_2|)^2\} \\ &= \int_0^{+\infty} \int_0^{+\infty} (x + y)^2 \times \frac{4x}{\sigma^2} e^{-\frac{2x}{\sigma^2}} \times \frac{4y}{\sigma^2} e^{-\frac{2y}{\sigma^2}} dx dy \\ &= \int_0^{+\infty} \frac{4x^3}{\sigma^2} e^{-\frac{2x}{\sigma^2}} dx \times \int_0^{+\infty} \frac{4y}{\sigma^2} e^{-\frac{2y}{\sigma^2}} dy \\ &\quad + 2 \int_0^{+\infty} \frac{4x^2}{\sigma^2} e^{-\frac{2x}{\sigma^2}} dx \times \int_0^{+\infty} \frac{4y^2}{\sigma^2} e^{-\frac{2y}{\sigma^2}} dy \\ &\quad + \int_0^{+\infty} \frac{4x}{\sigma^2} e^{-\frac{2x}{\sigma^2}} dx \times \int_0^{+\infty} \frac{4y^3}{\sigma^2} e^{-\frac{2y}{\sigma^2}} dy \\ &= \frac{\sigma^2}{2} + \frac{\pi\sigma^2}{4} + \frac{\sigma^2}{2} = \left(1 + \frac{\pi}{4}\right) \sigma^2, \end{aligned} \quad (37)$$

with the values of the definite integrals $\int_0^{+\infty} \frac{4x}{\sigma^2} e^{-\frac{2x}{\sigma^2}} dx = 1$, $\int_0^{+\infty} \frac{4x^2}{\sigma^2} e^{-\frac{2x}{\sigma^2}} dx = \frac{\sigma}{2} \sqrt{\frac{\pi}{2}}$, and

$\int_0^{+\infty} \frac{4x^3}{\sigma^2} e^{-\frac{2x^2}{\sigma^2}} dx = \frac{\sigma^2}{2}$. Thus, for the two-path case, the average-SNR gain of the MA system over the FPA system is obtained as

$$\eta_2 = \frac{\max_{\mathbf{r} \in \mathcal{C}_r} \gamma_2(\mathbf{r})}{\gamma_2(\mathbf{r}_0)} = \frac{G_{\max,2}}{G_0} = 1 + \frac{\pi}{4}. \quad (38)$$

Furthermore, the CDF of the maximum channel gain for the two-path case can be derived as

$$\begin{aligned} F_2(t) &\triangleq \Pr \{ (|b_1| + |b_2|)^2 \leq t \} \\ &= \int_0^{\sqrt{t}} dx \int_0^{\sqrt{t-x}} \frac{4x}{\sigma^2} e^{-\frac{2x^2}{\sigma^2}} \times \frac{4y}{\sigma^2} e^{-\frac{2y^2}{\sigma^2}} dy \\ &= \int_0^{\sqrt{t}} \frac{4x}{\sigma^2} e^{-\frac{2x^2}{\sigma^2}} \times \left[1 - e^{-\frac{2(\sqrt{t-x})^2}{\sigma^2}} \right] dx \\ &= \int_0^{\sqrt{t}} \frac{4x}{\sigma^2} e^{-\frac{2x^2}{\sigma^2}} - \frac{4x}{\sigma^2} e^{-\frac{t}{\sigma^2}} e^{-\frac{(2x-\sqrt{t})^2}{\sigma^2}} dx \\ &= 1 - e^{-\frac{2t}{\sigma^2}} - e^{-\frac{t}{\sigma^2}} \int_0^{\sqrt{t}} \frac{4x}{\sigma^2} e^{-\frac{(2x-\sqrt{t})^2}{\sigma^2}} dx \\ &= 1 - e^{-\frac{2t}{\sigma^2}} - \frac{2\sqrt{\pi t}}{\sigma} e^{-\frac{t}{\sigma^2}} \int_0^{\sqrt{2t}} \frac{1}{\sqrt{2\pi}\sigma} e^{-\frac{x^2}{2\sigma^2}} dx, \\ &= 1 - e^{-\frac{2t}{\sigma^2}} - \frac{\sqrt{\pi t}}{\sigma} e^{-\frac{t}{\sigma^2}} \left[1 - 2Q \left(\frac{\sqrt{2t}}{\sigma} \right) \right], \quad t \geq 0. \end{aligned} \quad (39)$$

with $Q(t) = \int_t^{+\infty} \frac{1}{\sqrt{2\pi}} e^{-\frac{x^2}{2}} dx$ being the Gaussian tail probability. For any given transmit power p_t , noise power δ^2 , and receive SNR threshold γ_{th} , the outage probability for the MA system with two receive paths is given by $F_2(\frac{\delta^2 \gamma_{\text{th}}}{p_t})$.

3) *Three-Path Case:* For any given $\varphi_{r,1}, \varphi_{r,2}, \varphi_{r,3}, \vartheta_{r,1}, \vartheta_{r,2}, \vartheta_{r,3}$, the maximum channel gain $(|b_1| + |b_2| + |b_3|)^2$ can always be achieved if the diameter of the receive region is larger than d_3 as shown in (28). Since b_ℓ is a CSCG random variable with mean zero and variance σ^2/L_r , $|b_\ell|$ is Rayleigh distributed with the PDF given by

$$f_{|b_\ell|}(t) = \frac{6t}{\sigma^2} e^{-\frac{3t^2}{\sigma^2}}, \quad t \geq 0, \quad \ell = 1, 2, 3, \quad (40)$$

Thus, as the size of the receive region approaches infinity, the upper bound on the maximum channel gain can always be achieved for arbitrary AoAs. The expected value of the maximum

channel gain of the MA in the receive region is thus given by

$$\begin{aligned}
G_{\max,3} &= \mathbb{E} \{ (|b_1| + |b_2| + |b_3|)^2 \} \\
&= \int_0^{+\infty} \int_0^{+\infty} \int_0^{+\infty} (x + y + z)^2 \times \frac{6x}{\sigma^2} e^{-\frac{3x^2}{\sigma^2}} \times \frac{6y}{\sigma^2} e^{-\frac{3y^2}{\sigma^2}} \times \frac{6z}{\sigma^2} e^{-\frac{3z^2}{\sigma^2}} dx dy dz \\
&= 3 \int_0^{+\infty} \frac{6x^3}{\sigma^2} e^{-\frac{3x^2}{\sigma^2}} dx \times \int_0^{+\infty} \frac{6y}{\sigma^2} e^{-\frac{3y^2}{\sigma^2}} dy \times \int_0^{+\infty} \frac{6z}{\sigma^2} e^{-\frac{3z^2}{\sigma^2}} dz \\
&\quad + 6 \int_0^{+\infty} \frac{6x^2}{\sigma^2} e^{-\frac{3x^2}{\sigma^2}} dx \times \int_0^{+\infty} \frac{6y^2}{\sigma^2} e^{-\frac{3y^2}{\sigma^2}} dy \times \int_0^{+\infty} \frac{6z}{\sigma^2} e^{-\frac{3z^2}{\sigma^2}} dz \\
&= 3 \times \frac{\sigma^2}{3} + 6 \times \frac{\pi\sigma^2}{12} = \left(1 + \frac{\pi}{2}\right) \sigma^2,
\end{aligned} \tag{41}$$

with the values of the definite integrals $\int_0^{+\infty} \frac{6x}{\sigma^2} e^{-\frac{3x^2}{\sigma^2}} dx = 1$, $\int_0^{+\infty} \frac{6x^2}{\sigma^2} e^{-\frac{3x^2}{\sigma^2}} dx = \frac{\sigma}{\sqrt{6}} \sqrt{\frac{\pi}{2}}$, and $\int_0^{+\infty} \frac{6x^3}{\sigma^2} e^{-\frac{3x^2}{\sigma^2}} dx = \frac{\sigma^2}{3}$. Thus, for the three-path case, the average-SNR gain of the MA system over the FPA system is obtained as

$$\eta_3 = \frac{\max_{\mathbf{r} \in \mathcal{C}_r} \gamma_3(\mathbf{r})}{\gamma_3(\mathbf{r}_0)} = \frac{G_{\max,3}}{G_0} = 1 + \frac{\pi}{2}. \tag{42}$$

Note that the maximum channel gain is the square-sum of three i.i.d. Rayleigh random variables, which has no closed-form CDF. Nevertheless, the CDF of the maximum channel gain for the three-path case can be approximated as [26]

$$\begin{aligned}
F_3(t) &\triangleq \Pr \{ (|b_1| + |b_2| + |b_3|)^2 \leq t \} = \Pr \{ |b_1| + |b_2| + |b_3| \leq \sqrt{t} \} \\
&\approx 1 - e^{-\frac{t}{c_3}} \left(1 + \frac{t}{c_3} + \frac{t^2}{2c_3^2} \right), \quad t \geq 0,
\end{aligned} \tag{43}$$

with $c_3 = \frac{15^{1/3}\sigma^2}{L_r}$. For any given transmit power p_t , noise power δ^2 , and receive SNR threshold γ_{th} , the outage probability for the MA system with three receive paths is approximately given by $F_3\left(\frac{\delta^2\gamma_{\text{th}}}{p_t}\right)$.

4) *Multiple-Path Case:* Since the EPRV \mathbf{b} is a CSCG random vector following distribution $\mathbf{b} \sim \mathcal{CN}(\mathbf{0}, \frac{\sigma^2}{L_r} \mathbf{I}_{L_r})$, the amplitude of the ℓ -th element of \mathbf{b} , i.e., $|b_\ell|$, is i.i.d. Rayleigh distributed with the PDF given by

$$f_{|b_\ell|}(t) = \frac{2L_r t}{\sigma^2} e^{-\frac{L_r t^2}{\sigma^2}}, \quad t \geq 0, \quad 1 \leq \ell \leq L_r, \tag{44}$$

If the number of receive paths is larger than three, it is difficult to derive the explicit expression of the maximum channel gain. Nevertheless, we can always obtain an upper bound on the maximum

channel gain of the MA as follows:

$$\begin{aligned}
G_{\max, L_r} &\leq \mathbb{E} \left\{ \left(\sum_{\ell=1}^{L_r} |b_\ell| \right)^2 \right\} \\
&= \int \cdots \int_0^{+\infty} \left(\sum_{\ell=1}^{L_r} x_\ell \right)^2 \times \prod_{\ell=1}^{L_r} \frac{2L_r x_\ell}{\sigma^2} e^{-\frac{L_r x_\ell^2}{\sigma^2}} dx_1 \cdots dx_{L_r} \\
&= L_r \int_0^{+\infty} \frac{2L_r x^3}{\sigma^2} e^{-\frac{L_r x^2}{\sigma^2}} dx + L_r(L_r - 1) \int_0^{+\infty} \frac{2L_r x}{\sigma^2} e^{-\frac{L_r x^2}{\sigma^2}} dx \times \int_0^{+\infty} \frac{2L_r y^3}{\sigma^2} e^{-\frac{L_r y^2}{\sigma^2}} dy \\
&= \frac{\sigma^2}{L_r} \times L_r + \frac{\pi \sigma^2}{4L_r} \times L_r(L_r - 1) = \left[1 + \frac{(L_r - 1)\pi}{4} \right] \sigma^2,
\end{aligned} \tag{45}$$

with the values of the definite integrals $\int_0^{+\infty} \frac{2L_r x}{\sigma^2} e^{-\frac{L_r x^2}{\sigma^2}} dx = 1$, $\int_0^{+\infty} \frac{2L_r x^2}{\sigma^2} e^{-\frac{L_r x^2}{\sigma^2}} dx = \frac{\sigma}{\sqrt{2L_r}} \sqrt{\frac{\pi}{2}}$, and $\int_0^{+\infty} \frac{2L_r x^3}{\sigma^2} e^{-\frac{L_r x^2}{\sigma^2}} dx = \frac{\sigma^2}{L_r}$. Hence, for the multiple-path case, the average-SNR gain of the MA system over the FPA system is upper-bounded by

$$\eta_{L_r} = \frac{\max_{\mathbf{r} \in \mathcal{C}_r} \gamma_{L_r}(\mathbf{r})}{\gamma_{L_r}(\mathbf{r}_0)} = \frac{G_{\max, L_r}}{G_0} \leq 1 + \frac{(L_r - 1)\pi}{4}. \tag{46}$$

Note that the CDF of the square-sum of L_r independent Rayleigh random variables has no closed-form expression for $L_r > 3$. Nevertheless, the CDF of the upper bound on the maximum channel gain for the multiple-path case can be obtained by the small argument approximation as follows [26]:

$$\begin{aligned}
F_{L_r}^{\text{UB}}(t) &\triangleq \Pr \left\{ \left(\sum_{\ell=1}^{L_r} |b_\ell| \right)^2 \leq t \right\} = \Pr \left\{ \sum_{\ell=1}^{L_r} |b_\ell| \leq \sqrt{t} \right\} \\
&\approx 1 - e^{-\frac{t}{c}} \sum_{k=0}^{L_r-1} \frac{\left(\frac{t}{c}\right)^k}{k!}, \quad t \geq 0,
\end{aligned} \tag{47}$$

with $c = \frac{\sigma^2}{L_r} [(2L_r - 1)!!]^{1/L_r}$ and $(2L_r - 1)!! = (2L_r - 1) \times (2L_r - 3) \times \cdots \times 3 \times 1$. For any given transmit power p_t , noise power δ^2 , and receive SNR threshold γ_{th} , a lower bound on the outage probability of the MA system with $L_r > 3$ receive paths is approximately given by $F_{L_r}^{\text{UB}}\left(\frac{\delta^2 \gamma_{\text{th}}}{p_t}\right)$.

5) *Infinite-Path Case*: For the isotropic scattering scenario, the number of receive paths approaches infinity with the joint PDF for the physical AoAs given by (12b). According to the central limit theorem, the channel coefficient at each position is a CSCG random variable with mean zero and variance σ^2 . Let $b(\theta_r, \phi_r)$ denote the complex path-response coefficient corresponding to AoAs θ_r and ϕ_r , which has an average power of σ^2 . The correlation between

the channel coefficients of two positions spaced by d can be derived as³

$$\begin{aligned} R(d) &= \mathbb{E} \{h^*(0, d)h(0, 0)\} = \mathbb{E} \left\{ \int_{-\pi/2}^{\pi/2} \int_{-\pi/2}^{\pi/2} |b(\theta_r, \phi_r)|^2 e^{j2\pi \frac{d}{\lambda} \sin \theta_r \frac{\cos \theta_r}{2\pi}} d\theta_r d\phi_r \right\} \\ &= \int_{-\pi/2}^{\pi/2} \sigma^2 e^{j2\pi \frac{d}{\lambda} \sin \theta_r \frac{\cos \theta_r}{2}} d\theta_r = \int_{-1}^1 \frac{\sigma^2}{2} e^{j2\pi \frac{d}{\lambda} t} dt = \sigma^2 \frac{\sin \left(2\pi \frac{d}{\lambda}\right)}{2\pi \frac{d}{\lambda}} = \sigma^2 \text{sinc} \left(\frac{2d}{\lambda}\right). \end{aligned} \quad (48)$$

According to the property of the sinc function, we know that the channels of two positions spaced by $\lambda/2$ are statistically independent. Due to the small value of $\text{sinc}(t)$ for $t \geq 1$, we can further assume that the channels of two positions with distance larger than $\lambda/2$ are statistically independent. Thus, for a square receive region with size $A \times A$, the number of independent random channel variables is no smaller than $N_{\text{LB}} = \lfloor 2A/\lambda + 1 \rfloor^2$. Since the channel coefficients are CSCG random variables, the channel (power) gains are exponential random variables (ERVs) with the rate parameter $1/\sigma^2$. The maximum channel gain of the MA in the receive region is lower-bounded by the largest order statistics of the N_{LB} independent ERVs, which can be expressed as $X_{\text{max}} = \max_{1 \leq k \leq N_{\text{LB}}} X_k$ with $\{X_k\}$ being i.i.d. ERVs with the rate parameter $1/\sigma^2$. It is known that the largest order statistics for i.i.d. ERVs can be equivalently expressed as $X_{\text{max}} = \sum_{k=1}^{N_{\text{LB}}} Y_k$, where $\{Y_k\}$ are independent ERVs with the rate parameter k/σ^2 for Y_k , $1 \leq k \leq N_{\text{LB}}$ [27]. Thus, the expected value for the lower bound on the maximum channel gain in the $A \times A$ area is obtained as

$$G_{\text{max}, \infty} \geq \mathbb{E} \left\{ \max_{1 \leq k \leq N_{\text{LB}}} X_k \right\} = \mathbb{E} \left\{ \sum_{k=1}^{N_{\text{LB}}} Y_k \right\} = \sum_{k=1}^{N_{\text{LB}}} \frac{\sigma^2}{k}, \quad (49)$$

which monotonously increases with the size of the receive region and approaches infinity for an infinite region. Besides, the CDF of the lower bound on the maximum channel gain for the infinite-path case is given by

$$F_{\infty}^{\text{LB}}(t) = \Pr \left\{ \max_{1 \leq k \leq N_{\text{LB}}} X_k \leq t \right\} = \left(1 - e^{-\frac{t}{\sigma^2}} \right)^{N_{\text{LB}}}. \quad (50)$$

Thus, for any given transmit power p_t , noise power δ^2 , and receive SNR threshold γ_{th} , an upper bound on the outage probability for the MA system with infinite number of receive paths is given by $F_{\infty}^{\text{LB}}\left(\frac{\delta^2 \gamma_{\text{th}}}{p_t}\right)$.

³Without loss of generality, the two positions spaced by d are selected along axis y_r . For any other two locations in the receive region with spacing d , we can always establish a new Cartesian coordinate system with the two points located on axis y_r , and the distribution of the corresponding AoAs does not change due to the assumption of isotropic scattering.

To analyze the upper bound on the maximum channel gain of the MA, we discretize the square receive region $A \times A$ into equally spaced grids with size $1/P \times 1/P$, and thus the total number of the grids is no larger than $N_{\text{UB}} = \lceil PA + 1 \rceil^2$. Let $\mathcal{C}_{r,k}$ denote the k -th grid in the receive region, $1 \leq k \leq N_{\text{UB}}$. Thus, the maximum channel gain of the MA in the $A \times A$ area can be equivalently expressed as

$$\max_{\mathbf{r} \in \mathcal{C}_r} |h(\mathbf{r})|^2 = \max_{1 \leq k \leq N} \max_{\mathbf{r} \in \mathcal{C}_{r,k}} |h(\mathbf{r})|^2. \quad (51)$$

For sufficiently large P , the area of each grid approaches zero such that the correlation between channels at any two points within the same grid approaches σ^2 . It indicates that the maximum channel gain over each grid can be approximately given by the channel gain at the center of this grid, i.e., $\max_{\mathbf{r} \in \mathcal{C}_{r,k}} |h(\mathbf{r})|^2 \cong \tilde{X}_k$ with $\{\tilde{X}_k\}$ being i.i.d. exponential variables with the rate parameter $1/\sigma^2$. Thus, an upper bound on the maximum channel gain can be obtained by assuming the channel gains at the center of the N grids are all statistically independent, i.e.,

$$G_{\text{max},\infty} \leq \mathbb{E} \left\{ \max_{1 \leq k \leq N_{\text{UB}}} \tilde{X}_k \right\} = \sum_{k=1}^{N_{\text{UB}}} \frac{\sigma^2}{k}. \quad (52)$$

Meanwhile, the CDF of the upper bound on the maximum channel gain is given by

$$F_{\infty}^{\text{UB}}(t) = \Pr \left\{ \max_{1 \leq k \leq N_{\text{UB}}} \tilde{X}_k \leq t \right\} = \left(1 - e^{-\frac{t}{\sigma^2}} \right)^{N_{\text{UB}}}. \quad (53)$$

Thus, for any given transmit power p_t , noise power δ^2 , and receive SNR threshold γ_{th} , a lower bound on the outage probability for the MA system with infinite number of receive paths is given by $F_{\infty}^{\text{UB}}\left(\frac{\delta^2 \gamma_{\text{th}}}{p_t}\right)$. It is known that the sum of the first N terms of the harmonic series can be approximated by $\sum_{k=1}^N \frac{1}{k} \approx \log N + \varsigma$, with $\varsigma \approx 0.577$ denoting the Euler-Mascheroni constant. Thus, the lower and upper bounds in (49) and (52) indicate that the expected value for the maximum channel gain in the receive region increases with the region size approximately following a logarithmic function.

IV. SIMULATION RESULTS

In this section, extensive simulations are carried out to evaluate the performance of the MA-enabled communication systems and verify our analytical results.

A. Simulation Setup and Benchmark Schemes

In the simulation, the position of the transmit antenna is fixed, while the receive MA can be moved flexibly in the receive region, which is set as a square area with size $A \times A$, i.e., $\mathcal{C}_r = [A/2, A/2] \times [A/2, A/2]$. The ratio of the average receive signal power to the noise power is set as $\frac{p_t \sigma^2}{\delta^2} = 1$ for convenience. The geometry channel model is employed as a special case of our proposed field-response based model, where the number of transmit and receive paths are the same, i.e., $L_t = L_r$, with a diagonal PRM $\Sigma = \text{diag}\{b_1, b_2, \dots, b_{L_r}\}$. The path-response coefficients are assumed to be i.i.d. CSCG random variables, i.e., $b_\ell \sim \mathcal{CN}(0, \sigma^2/L_r)$, $1 \leq \ell \leq L_r$. Besides, the physical AoDs and AoAs are assumed to be i.i.d. random variables with the PDF given by (12). For each channel realization, we employ exhaustive search for the position of the receive MA which achieves the highest channel gain. The results in this section are carried out based on 10^4 Monte Carlo simulations.

In addition to the proposed MA system, three benchmark schemes are defined as follows:

- FPA: The antenna at the Rx has a fixed position located at the reference point $\mathbf{r}_0 = (0, 0)$.
- AS: The Rx is equipped with 1 RF chain and an array with M antennas spaced by a half wavelength in the receive region. In particular, the antenna with the highest channel gain is selected out of the M antennas for maximizing the receive SNR.
- Digital beamforming (DBF): In the SIMO system, the Rx is equipped with M RF chains and an array with M antennas spaced by a half wavelength in the receive region. In particular, the MRC is employed at the Rx for maximizing the receive SNR.

For all the schemes, we define the the relative SNR gain as the ratio of the SNR for the considered scheme to the SNR for the scheme with a single transmit FPA at \mathbf{t}_0 and a single receive FPA at \mathbf{r}_0 .

B. Numerical Results

Fig. 7 shows the relative SNR gains for MA, AS, and DBF systems with varying normalized size of the receive region. The number of receive paths is set as $L_r = 2$, $L_r = 3$, and $L_r = 5$ for the three subplots, respectively. As can be observed, the relative SNR gain of the MA system increases with the region size because a higher maximum channel gain can be found in a larger receive region. The analytical upper bounds on the relative SNR gain are given by (38), (42), and (46). It can be seen that for the two-path and three-path cases, the upper bounds provided by

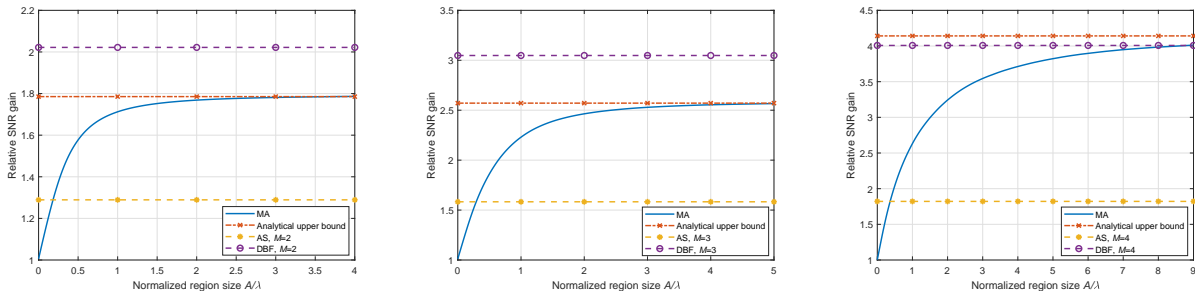


Fig. 7. Comparison of the relative SNR gains for MA, AS, and DBF systems versus the normalized size of the receive region with the number of receive paths $L_r = 2$, $L_r = 3$, and $L_r = 5$, respectively.

(38) and (42) are tight due to the strong periodicity of the channel gain. The minimum size of the receive region for achieving the upper bound on the relative SNR gain is 4λ and 5λ for $L_r = 2$ and $L_r = 3$, respectively. This result is consistent with the derivation in (20) and (28), where a larger size of the region is required to guarantee achieving the upper bound on the maximum channel gain as the number of receive paths increases. This conclusion can be further verified by the case of $L_r = 5$, where the relative SNR gain still increases if the region size is larger than 8λ . The reason is that as the number of paths increases, the periodicity becomes weaker in the receive region. According to the period analysis in (32), the maximal common factor for the virtual AoA indices decreases with the number of paths, which entails a larger period for the channel gain in the receive region. Thus, to achieve the upper bound on the relative SNR gain, a larger size of the receive region is required for the case of more paths. Besides, the relative SNR gains of AS and DBF systems are also evaluated in Fig. 7. As can be observed, although the number of antennas for AS and DBF systems is M times larger than that for the MA system, the MA system can achieve a performance comparable to that of the DBF system and better than that of the AS system. For the AS system, the relative SNR gain is small because the candidate antennas have fixed positions. In contrast, the MA system has more flexibility to adjust the position of the antenna for achieving a higher SNR. It can be expected that the AS scheme can approach the performance of the MA system if a sufficiently large number of antennas are employed at the Rx. However, this will result in much higher hardware cost, where the entire receive region should be covered by antennas. For the DBF system, the array/MRC gain increases more significantly with the number of antennas as compared to AS. However, the number of RF chains increases with the number of antennas, and thus the hardware cost for the DBF system is larger than that for the MA/AS system.

Fig. 8 compares the SNR CDFs for MA, FPA, AS, and DBF systems with the same setup

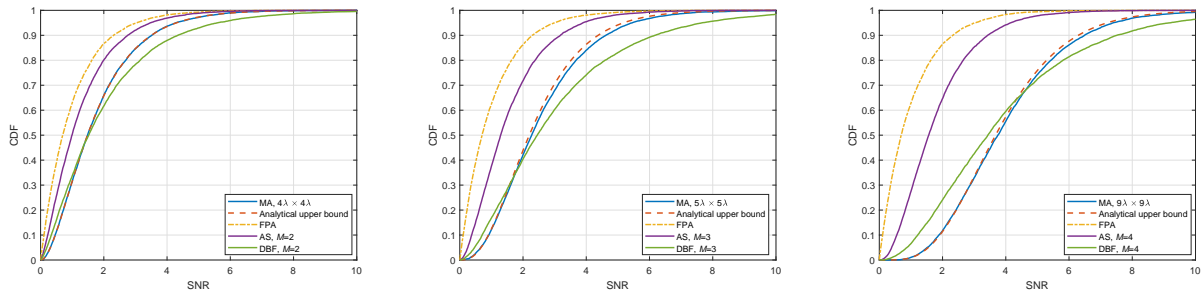


Fig. 8. Comparison of the SNR CDFs for MA, FPA, AS, and DBF systems with the number of receive paths $L_r = 2$, $L_r = 3$, and $L_r = 5$, respectively.

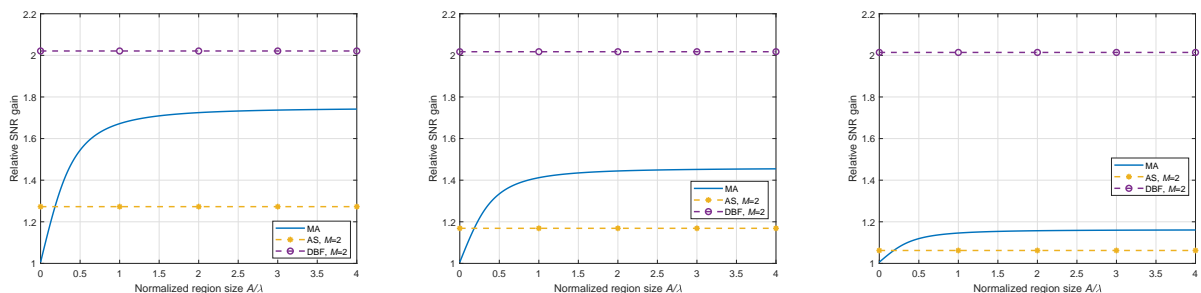


Fig. 9. Comparison of the relative SNR gains for MA, AS, and DBF systems versus the normalized size of the receive region with $L_r = 2$ and the ratio of average path power $\rho = 2$, $\rho = 10$, and $\rho = 100$, respectively.

as Fig. 7. As can be observed, the simulated CDF of the SNR for the two-path MA system perfectly matches the analytical result derived in (39). While for the $L_r = 3$ and $L_r = 5$ cases, the simulated CDF has a deviation compared to the analytical ones because an approximation was employed in (43) and (47). Nevertheless, the error between the analytical and simulated CDFs is very small, which indicates that (43) and (47) provide a good approximation for the CDF of the upper bound on the maximum channel gain and can be utilized for analyzing the outage probability for the MA system. Besides, we can find that for any fixed SNR threshold, the value of the CDF for the MA system is always smaller than that for FPA and AS systems, which means that compared to the two benchmark schemes, the MA system can always achieve a lower outage probability for any SNR threshold. Interestingly, at the low SNR region, the SNR CDF value for the MA system is smaller than that for the DBF system. It indicates that the MA system can outperform the DBF system in terms of the outage probability at the low SNR region. In particular, for a large number of receive paths, the performance gap of the outage probability increases, which shows more superiority of the MA system.

The analytical and simulated results so far are all based on the assumption that the variances of the path-response coefficients $\{b_\ell\}$ are the same for different channel paths, which yields the

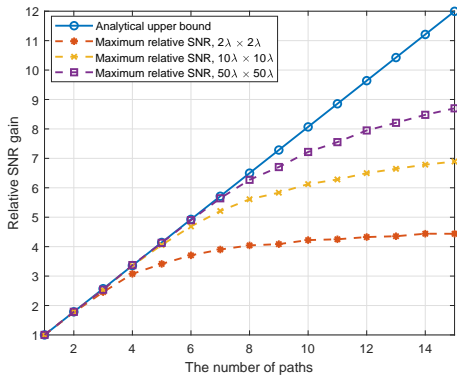


Fig. 10. The expected values of the relative SNR gains for MA systems versus the number of receive paths for different sizes of the receive region.

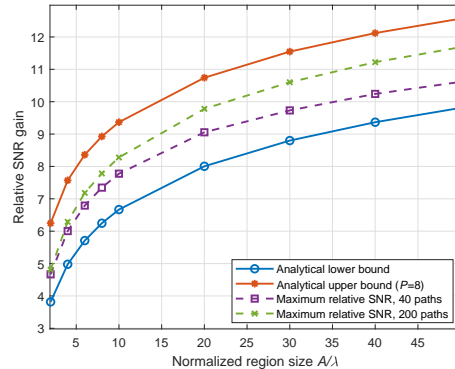


Fig. 11. The expected values of the relative SNR gains versus the normalized size of the receive region for different numbers of receive paths.

same average power of the multi-path components. In Fig. 9, we evaluate the relative SNR gains for MA, AS, and DBF systems with different ratios of the average path power. Specifically, the number of paths is set as $L_r = 2$, and the ratio of the average power for the two paths, denoted by $\rho = \frac{\mathbb{E}\{|b_1|^2\}}{\mathbb{E}\{|b_2|^2\}}$, is set as 2, 10, and 100 for the three subplots, respectively. It can be observed again that the relative SNR gain of MA increases with the region size. However, as the ratio of the path power increases, the increment of the relative SNR gains provided by the MA and AS systems both decreases. For $\rho = 2$, $\rho = 10$, and $\rho = 100$, the increment of the relative SNR gain is 0.74, 0.45, and 0.16, respectively. The reason is as follows. The SNR gain of the MA system is essentially obtained from the small-scale fading of the multi-path channel. For a large number of paths with equal average power, the small-scale fading becomes strong because the fluctuation of the channel gain caused by the phase change of the electromagnetic waves is substantial in the receive region. As the ratio of the path power increases, the difference of the maximum and minimum channel gains in the receive region decreases, and thus the relative SNR gain provided by adjusting the position of the MA decreases. For an extreme case with the ratio of the path power approaching infinity, the channel is degraded to the single-path case, where no SNR gain can be obtained by the MA system over the FPA system as we have shown in Section III-A.

In Fig. 10, we compare the relative SNR gain and the upper bound on the maximum SNR gain for the MA system with varying number of receive paths. As can be observed, both the relative SNR gain and the upper bound on the maximum SNR gain increase with the number of paths. This is because the small-scale fading becomes stronger as the number of paths increases, and thus the channel gain has more substantial fluctuation in the receive region, which entails

an increase on the maximum channel gain. Besides, as the region size increases from $2\lambda \times 2\lambda$ to $50\lambda \times 50\lambda$, the maximum SNR gain closely approaches the analytical upper bound provided by (46). In particular, if the number of paths is smaller than 3, the performance gap between the maximum SNR gain for $2\lambda \times 2\lambda$ region and the upper bound is no more than 0.12. If the number of paths is smaller than 5, the performance gap between the maximum SNR gain for $10\lambda \times 10\lambda$ region and the upper bound is no more than 0.10. If the number of paths is smaller than 7, the performance gap between the maximum SNR gain and the upper bound is no more than 0.08. The above results indicate that the upper bound in (46) is approximately tight for a small number of paths. For larger number of paths, a larger size of the receive region is required to achieve the SNR performance near to the upper bound. It is worth noting that the upper bound is effective for infinite size of the receive region. It is expected that the maximum SNR gain can further increase if the size of the receive region is larger than $50\lambda \times 50\lambda$ and approach the upper bound for infinitely large size of the receive region more closely.

Finally, Fig. 11 shows the expected value of the relative SNR gain versus the normalized size of the receive region as well as the comparison with the lower and upper bounds in (49) and (52). The number of paths is set as 40 or 200, and the discretized parameter for the upper bound is set as $P = 8$ in (52). As can be observed, the relative SNR gains increase with the size of the region, and the performance gap to the upper bound decreases if the number of paths increases. As we have analyzed in Section III-B, the lower and upper bounds in (49) and (52) both approximately follow a logarithmic function with the region size. The results in Fig. 11 validate this analysis and show that the relative SNR gains for sufficiently large number of paths have a logarithmic growth with respect to the size the receive region.

V. CONCLUSION

In this paper, we proposed a new MA architecture for improving the performance of wireless communication systems. With the capability of flexible movement, the MAs can be deployed at positions with more favorable channel conditions in the spatial region to achieve higher spatial diversity gains. Since the channel varies with the positions of the MAs, a field-response based channel model was developed under the far-field condition to characterize the general multi-path channel with given transmit and receive regions. We have shown the conditions under which the proposed field-response based channel model for MAs becomes the well-known LoS channel, geometry channel, Rayleigh and Rician fading channel models with FPAs. Based on the proposed channel model, we analyzed the maximum channel gain achieved by a single receive MA over its

FPA counterpart under both deterministic and stochastic channels. In the deterministic channel case, the periodic behavior of the multi-path channel gain was revealed in a given spatial field, which unveiled the maximum channel gain of the MA with respect to the number of channel paths and size of the receive region. In the case of stochastic channels, we derived the expected value of an upper bound on the maximum channel gain of the MA in an infinitely large receive region for different numbers of channel paths. Moreover, our results revealed that higher performance gains by the MA over the FPA could be acquired when the number of channel paths increases due to more pronounced small-scale fading effects in the spatial domain. Besides, for uniform scattering scenarios with infinite number of channel paths, we showed that the upper and lower bounds on the expected maximum channel gain of the MA obey the logarithmic increase with respect to the size of the receive region. The approximate CDF of the maximum channel gain was also obtained in closed form, which is useful to evaluate the outage probability of the MA system. Simulation results validated our analytical results and demonstrated that the MA system could reap considerable performance gains over the conventional FPA systems with/without AS, and even achieve comparable performance to the SIMO beamforming system. With the general channel model and theoretical performance limits of the MA system provided in this paper, the design of practical methods for achieving the performance limits, such as channel estimation and antenna position searching algorithms, as well as the extension of the results to multi-antenna/multi-user systems with spatial multiplexing will be interesting topics for future research.

REFERENCES

- [1] E. Telatar, "Capacity of multi-antenna gaussian channels," *European Trans. Telecommun.*, vol. 10, no. 6, pp. 585–595, Nov. 1999.
- [2] A. Paulraj, D. Gore, R. Nabar, and H. Bolcskei, "An overview of MIMO communications - a key to gigabit wireless," *Proceedings of the IEEE*, vol. 92, no. 2, pp. 198–218, Feb. 2004.
- [3] G. Stuber, J. Barry, S. McLaughlin, Y. Li, M. Ingram, and T. Pratt, "Broadband MIMO-OFDM wireless communications," *Proceedings of the IEEE*, vol. 92, no. 2, pp. 271–294, Feb. 2004.
- [4] L. Lu, G. Y. Li, A. L. Swindlehurst, A. Ashikhmin, and R. Zhang, "An overview of massive MIMO: Benefits and challenges," *IEEE J. Sel. Topics Signal Process.*, vol. 8, no. 5, pp. 742–758, Oct. 2014.
- [5] E. G. Larsson, O. Edfors, F. Tufvesson, and T. L. Marzetta, "Massive MIMO for next generation wireless systems," *IEEE Commun. Mag.*, vol. 52, no. 2, pp. 186–195, Feb. 2014.
- [6] B. Ning, Z. Tian, Z. Chen, C. Han, J. Yuan, and S. Li, "Prospective beamforming technologies for ultra-massive MIMO in terahertz communications: A tutorial," *arXiv preprint arXiv:2107.03032*, 2021.
- [7] X. Shao, C. You, W. Ma, X. Chen, and R. Zhang, "Target sensing with intelligent reflecting surface: Architecture and performance," *IEEE J. Select. Areas Commun.*, vol. 40, no. 7, pp. 2070–2084, Jul. 2022.

- [8] Y. Zeng and R. Zhang, "Millimeter wave MIMO with lens antenna array: A new path division multiplexing paradigm," *IEEE Trans. Commun.*, vol. 64, no. 4, pp. 1557–1571, Apr. 2016.
- [9] L. Zhu, J. Zhang, Z. Xiao, X. Cao, D. O. Wu, and X.-G. Xia, "Millimeter-wave NOMA with user grouping, power allocation and hybrid beamforming," *IEEE Trans. Wireless Commun.*, vol. 18, no. 11, pp. 5065–5079, Nov. 2019.
- [10] B. Ning, Z. Chen, W. Chen, and J. Fang, "Beamforming optimization for intelligent reflecting surface assisted MIMO: A sum-path-gain maximization approach," *IEEE Wireless Commun. Lett.*, vol. 9, no. 7, pp. 1105–1109, Jul. 2020.
- [11] C. Huang, S. Hu, G. C. Alexandropoulos, A. Zappone, C. Yuen, R. Zhang, M. D. Renzo, and M. Debbah, "Holographic MIMO surfaces for 6G wireless networks: Opportunities, challenges, and trends," *IEEE Wireless Commun.*, vol. 27, no. 5, pp. 118–125, Oct. 2020.
- [12] A. Pizzo, T. L. Marzetta, and L. Sanguinetti, "Spatially-stationary model for holographic MIMO small-scale fading," *IEEE J. Select. Areas Commun.*, vol. 38, no. 9, pp. 1964–1979, Sep. 2020.
- [13] A. Pizzo, L. Sanguinetti, and T. L. Marzetta, "Fourier plane-wave series expansion for holographic MIMO communications," *IEEE Trans. Wireless Commun.*, 2022 (Early Access).
- [14] Z. Zhang and L. Dai, "Pattern-division multiplexing for continuous-aperture MIMO," *arXiv Preprint arXiv:2203.14264*, 2022.
- [15] R. Deng, B. Di, H. Zhang, Y. Tan, and L. Song, "Reconfigurable holographic surface: Holographic beamforming for metasurface-aided wireless communications," *IEEE Trans. Veh. Technol.*, vol. 70, no. 6, pp. 6255–6259, Jun. 2021.
- [16] S. Hu, F. Rusek, and O. Edfors, "Beyond massive MIMO: The potential of data transmission with large intelligent surfaces," *IEEE Trans. Signal Process.*, vol. 66, no. 10, pp. 2746–2758, May 2018.
- [17] D. Castanheira and A. Gameiro, "Distributed antenna system capacity scaling," *IEEE Wireless Commun.*, vol. 17, no. 3, pp. 68–75, Jun. 2010.
- [18] R. Heath, S. Peters, Y. Wang, and J. Zhang, "A current perspective on distributed antenna systems for the downlink of cellular systems," *IEEE Commun. Mag.*, vol. 51, no. 4, pp. 161–167, Apr. 2013.
- [19] H. Cui and Y. Liu, "Green distributed antenna systems for smart communities: A comprehensive survey," *China Commun.*, vol. 16, no. 11, pp. 70–80, Nov. 2019.
- [20] A. Zhuravlev, V. Razevig, S. Ivashov, A. Bugaev, and M. Chizh, "Experimental simulation of multi-static radar with a pair of separated movable antennas," in *Proc. IEEE International Conf. Microwaves Commun. Antennas Electron. Syst. (COMCAS)*, Nov. 2015, pp. 1–5.
- [21] S. Basbug, "Design and synthesis of antenna array with movable elements along semicircular paths," *IEEE Antennas Wireless Propagat. Lett.*, vol. 16, pp. 3059–3062, Oct. 2017.
- [22] K.-K. Wong, A. Shojaeifard, K.-F. Tong, and Y. Zhang, "Fluid antenna systems," *IEEE Trans. Wireless Commun.*, vol. 20, no. 3, pp. 1950–1962, Mar. 2021.
- [23] K.-K. Wong and K.-F. Tong, "Fluid antenna multiple access," *IEEE Trans. Wireless Commun.*, vol. 21, no. 7, pp. 4801–4815, Jul. 2022.
- [24] A. Molisch and M. Win, "MIMO systems with antenna selection," *IEEE Microwave Mag.*, vol. 5, no. 1, pp. 46–56, Mar. 2004.
- [25] S. Sanayei and A. Nosratinia, "Antenna selection in MIMO systems," *IEEE Commun. Mag.*, vol. 42, no. 10, pp. 68–73, Oct. 2004.
- [26] J. Hu and N. Beaulieu, "Accurate simple closed-form approximations to Rayleigh sum distributions and densities," *IEEE Commun. Lett.*, vol. 9, no. 2, pp. 109–111, Feb. 2005.
- [27] V. K. Rohatgi and A. M. E. Saleh, *An introduction to probability and statistics*. Hoboken, New Jersey, USA: John Wiley & Sons, 2015.